Structural Characterization of the Interaction between TFIIIB Components Bdp1 and Brf1

Fakhri Saïda*,‡

Center for Molecular Genetics, University of California at San Diego, 9500 Gilman Drive, La Jolla, California 92093

Received July 27, 2008; Revised Manuscript Received October 5, 2008

ABSTRACT: Transcription factor TFIIIB plays key roles in transcription by RNA polymerase III. Its three components (TBP, Brf1, and Bdp1) participate in crucial molecular events that include RNA polymerase recruitment, formation of the open initiation complex, and recycling of transcription. Although the details of the interaction among DNA, TBP, and Brf1 have been, in part, revealed through the crystal structure of their ternary complex, structural details of the Brf1−Bdp1 interaction are lacking. In this paper, nuclear magnetic resonance (NMR) is used to map the interaction interface between Bdp1 and Brf1 at single-amino acid resolution, using minimal functional segments of the two proteins. An NMR-derived structural model shows that the principal anchorage site of Brf1 is located on a convex surface of Bdp1 that encompasses helix 1 and helix 3 of its conserved SANT domain. The main Bdp1 anchorage site is provided by a small set of residues belonging to a Brf1 segment of residues 470−495.

Transcription by RNA polymerase III (pol III) is a complex molecular process orchestrated by the two main transcription factors, TFIIIB and TFIIIC (*1*−*3*). TFIIIB is composed of three subunits: the TATA box-binding protein (TBP), the TFIIB-related factor (Brf1), and Bdp1. TBP is common to all three nuclear eukaryotic transcription systems and provides direct recognition of TATA boxes for a subset of pol III-transcribed *Saccharomyces cerevisiae* genes. Brf1, a bipartite protein of 596 amino acids, has an N-terminal part (residues 1−287) homologous to transcription factor TFIIB and a C-terminal part responsible for binding TBP (*4*). The 594-amino acid Bdp1 is specific to the pol III transcription system. Little is known about the molecular architecture of Bdp1 except the conservation (among fungi and humans) of its segment of amino acids 415−472 that contains the SANT (SWI3, ADA2, N-COR, and TFIIIB″) domain (*3, 5*).

A previous photochemical protein−DNA cross-linking analysis identified *S. cerevisiae* Brf1 residues 441−506 and Bdp1 residues 410−476 as the principal interaction site of these two proteins (*6*). In this work, I used NMR[1] to derive a high-resolution map of this interaction. For this purpose, I isolated a small protease-resistant C-proximal Bdp1 fragment that is compatible with NMR analysis, assigned the resonances of its backbone, and titrated its $^{15}N-^{1}H$ cross-peaks with unlabeled Brf1 to generate a map of the Brf1 anchorage site on Bdp1. Similarly, I assigned the backbone of Brf1 and titrated its $^{15}N-^{1}H$ cross-peaks with unlabeled Bdp1 to generate a map of the Bdp1 anchorage site on Brf1. A NMR-based model of the three-dimensional structure of this segment of Bdp1 shows the Brf1 anchorage site occupying a convex surface that covers helix 1 and helix 3 of the conserved SANT domain. The main Bdp1 anchorage site is provided by a particular set of residues belonging to the Brf1 segment of residues 470−495. On the crystal structure of a DNA−TBP−Brf1 ternary complex (*4*), this Bdp1 anchorage site overlaps with helices 24 and 25 of Brf1. An NMR experiment examining the effect of TBP on the conformation of Brf1 is briefly presented and discussed.

EXPERIMENTAL PROCEDURES

Proteins. Untagged Bdp1(245−537) was expressed at 37 °C in Luria broth medium and purified through selective ammonium sulfate precipitation (40%) followed by sequential ion-exchange chromatography on a 5 mL HiTrap Q HP column and a 5 mL HiTrap SP HP column (GE Healthcare). TBP(61−240) was expressed at 37 °C as a tandem fusion to an N-terminal hexahistidinyl tag followed by a hexaglycyl-seryl linker and a TEV protease cleavage site. The protein was first purified on nickel-Sepharose beads (GE Healthcare). Upon treatment with TEV protease, tagless TBP(61−240) was recovered after a chromatography step on a 5 mL HiTrap heparin HP column (GE Healthcare). Brf1(439−544) and the TBP(61−240)−$(GS)_6$−Brf1(439−544) fusion protein (both C-terminally His_6-tagged) were expressed and purified as described previously (*7*). Bdp1-(412−493), fused to a hexahistidinyl tag at its N-terminus, was expressed at 37 °C as inclusion bodies, purified on nickel-Sepharose beads in the presence of 6 M urea, and refolded through extensive dialysis against the renaturation buffer [20 mM sodium phosphate (pH 6.4), 500 mM NaCl, 50 mM arginine, 50 mM glutamic acid, 5 mM DTT, and 0.05% Tween 20].

Limited Proteolysis. Bdp1(245−537) (0.6 mg/mL) was digested with modified trypsin and chymotrypsin at a protease:Bdp1 mass ratio of 1:1000 (chymotrypsin) or 1:3000

* To whom correspondence may be addressed. E-mail: fsaida@biomail.ucsd.edu. Phone: (858) 729-4375. Fax: (858) 729-3455.

‡ Present address: General Atomics, 3550 General Atomics Ct., San Diego, CA 92121.

[1] Abbreviations: NMR, nuclear magnetic resonance; HSQC, heteronuclear single-quantum correlation; DTT, dithiothreitol; PMSF, phenylmethanesulfonyl fluoride; TCA, trichloroacetic acid.

10.1021/bi801406z CCC: $40.75
Published on Web 11/17/2008

(trypsin) in 50 mM Tris-HCl (pH 8), 1 mM $CaCl_2$, 0.7 mM $MgCl_2$, 0.5 mM DTT, and 100 mM NaCl. At regular time intervals, samples for SDS−PAGE analysis were placed into tubes providing 1× SDS−sample buffer with 10 mM PMSF and incubated for 5 min at 95 °C. Bdp1(412−537)-C-His_6 was digested with carboxypeptidase Y (1:20 protease:Bdp1 mass ratio) in 50 mM sodium phosphate (pH 6.4) and 150 mM NaCl at 25 °C, and digestion was stopped as described above. Protease-resistant fragments were gel-extracted and TCA-precipitated for the sole purpose of N-terminal sequencing. For mass spectrometric analysis, proteolysis was stopped by adding PMSF to a final concentration of 10 mM (at the peak of accumulation of the protease-resistant fragment), heating at 95 °C, and TCA precipitation. Samples were then analyzed on a PE Biosystems Voyager-DE STR MALDI-TOF spectrometer.

NMR. All NMR data were collected at 298 K on Bruker DRX-600 (equipped with a 5 mm triple-resonance indirect cryoprobe) and DRX-800 spectrometers. ^{15}N and ^{13}C uniform isotopic labeling of Bdp1 and Brf1 was conducted according to a previously published protocol (*8*). Typical NMR protein samples were 0.3−0.6 mM in NMR buffer [20 mM sodium phosphate (pH 6.4), 200 mM NaCl, 50 mM arginine, 50 mM glutamic acid, 5 mM DTT, 0.5 mM EDTA, 0.4 mM PMSF, and 10% D_2O]. Bdp1 and Brf1 backbone resonance assignments were determined by means of HNCA, HN(CO)CA, HNCACB, CBCA(CO)NH, HNCO, HNHA, and $^{15}N-^{1}H$ HSQC experiments. Proton chemical shifts were referred to the methyl ^{1}H resonance frequency of 2,2-dimethyl-2-silapentane-5-sulfonic acid. ^{13}C and ^{15}N resonances were indirectly calibrated according to IUPAC recommendations (*9*). Data were processed using XWINNMR 3.0 (Bruker) and analyzed using SPARKY 3.11 (T. D. Goddard and D. G. Kneller, University of California, San Francisco). MARS 1.1.3 (*10*) was used for the semiautomatic sequential assignment of both Bdp1 and Brf1. Secondary structures of Bdp1 and Brf1 were derived using the chemical shift index of the $^{1}H^{\alpha}$, $^{13}C^{\alpha}$, $^{13}C^{\beta}$, and $^{13}C'$ nuclei (CSI 2.1) (*11*). The secondary structure of Brf1 was recomputed by directly calculating the secondary chemical shift of $^{13}C'$, which includes sequence-dependent corrections of random coil NMR chemical shifts (*12*). A Perl script calculating these corrections was generously provided by K.-P. Wu (Rutgers University, New Brunswick, NJ). NMR titration experiments consisted of a series of HSQC spectra with identical acquisition and processing parameters. The reference spectrum corresponded to that of the free ^{15}N-labeled protein in the NMR buffer. For the HSQC spectral titration, small volumes of concentrated, unlabeled ligand that had been extensively dialyzed against NMR buffer were added. Dilution factors were negligible (<10%). ^{15}N and ^{1}H chemical shift perturbations, Δ, were quantified using the relationship $\Delta = [(\delta\sigma_H)^2 + (\delta\sigma_N/10)^2]^{1/2}$, where $\delta\sigma_H$ and $\delta\sigma_N$ are changes, in parts per million, of the proton and nitrogen chemical shifts, respectively. Although this yields smaller values for chemical shift perturbation compared to the widely used formula $\{\Delta = [(\delta\sigma_H)^2 + (\delta\sigma_N/5)^2]^{1/2}\}$ (*13*), it more evenly weights changes in the proton and nitrogen dimensions. A model of the three-dimensional structure of Bdp1 was generated by threading the experimentally measured backbone chemical shifts into a structural ensemble of proteins that are less than 25% identical in sequence with Bdp1 [Thrifty 1.0 (*14*)]. The validity of the model obtained was assessed using VADAR 1.5 (Volume, Area, Dihedral Angle Reporter) (*15*).

Brf1/Bdp1 Pull-Down Assay. One milliliter of 20 mM sodium phosphate (pH 6.4), 200 mM NaCl, 50 mM arginine, 50 mM glutamic acid, and 5 mM DTT containing 25 μM Bdp1(412−493) and either 26, 65, or 130 μM Brf1(439−544) was incubated at 25 °C for 15 min and added to 200 μL of heparin Sepharose (equilibrated in the same buffer) with continuous mixing for an additional 15 min. The beads were sedimented for 10 s at 2000*g*, and the supernatant material was recovered (fraction FT). The beads were resuspended in 1 mL of the same buffer and sedimented three times (fractions W1, W2, and W3) followed by two elutions with 1 mL of the same buffer containing 1 M NaCl (fractions E1 and E2). A 10 μL aliquot of each supernatant fraction was analyzed by SDS−PAGE.

RESULTS

Limited Proteolysis of the C-Terminus of Bdp1. To identify a suitably small C-terminal domain of Bdp1 that would be compatible with NMR analysis, Bdp1(245−537) was subjected to controlled proteolysis with trypsin and chymotrypsin (*16, 17*). Protease-resistant fragments were identified by N-terminal sequencing and mass spectrometry. Preliminary mapping with trypsin yielded a major resistant fragment identified as Bdp1 residues 319−537 (see Figure 1A, left panel, 30 min time point). Several smaller fragments were also observed over time, suggesting that Bdp1(319−537) might be composed of smaller subdomains.

Chymotrypsin digestion of Bdp1(245−537) yielded a single, very stable, fragment identified as Bdp1 residues 412−537 (Figure 1A, right panel). Bdp1(412−537) containing a C-terminal His_6 tag was expressed in *Escherichia coli* and purified under native conditions. Digestion of this protein from the C-terminal end with carboxypeptidase Y (Figure 1B, left panel) yielded a highly resistant fragment after overnight digestion similar in size to a trypsin cleavage product of the same protein (right panel), identified as Bdp1 residues 412−490. Figure 1C specifies all identified cleavage sites of Bdp1(245−537).

The protease-resistant Bdp1(412−490) was chosen for structural characterization by NMR. This fragment contains the SANT domain and the major interaction interface between TFIIIB components Bdp1 and Brf1 (*6*).

Backbone Assignment and Secondary Structure of Bdp1. Bdp1(412−493) containing three additional C-terminal residues and a His_6 tag was uniformly labeled with ^{13}C and ^{15}N, purified under denaturing conditions, renatured, and assigned using multidimensional NMR (see Experimental Procedures). Secondary structure was derived using the chemical shift index of $^{1}H^{\alpha}$, $^{13}C^{\alpha}$, $^{13}C^{\beta}$, and $^{13}C'$ (*11*). Figure 2A shows that this fragment folds into three helices: α1 (residues T421−G436), α2 (residues S443−Y446), and α3 (residues S450−K464).

Figure 2B compares the secondary structure of Bdp1(412−493) with five SANT domain representatives of known structure. The level of sequence identity of the Bdp1 SANT domain with these five representatives ranged from 32% (2CU7; human histone H2A deubiquitinase) to 12% (2ELK; *Schizosaccharomyces pombe* Ada2). The location of the three helices

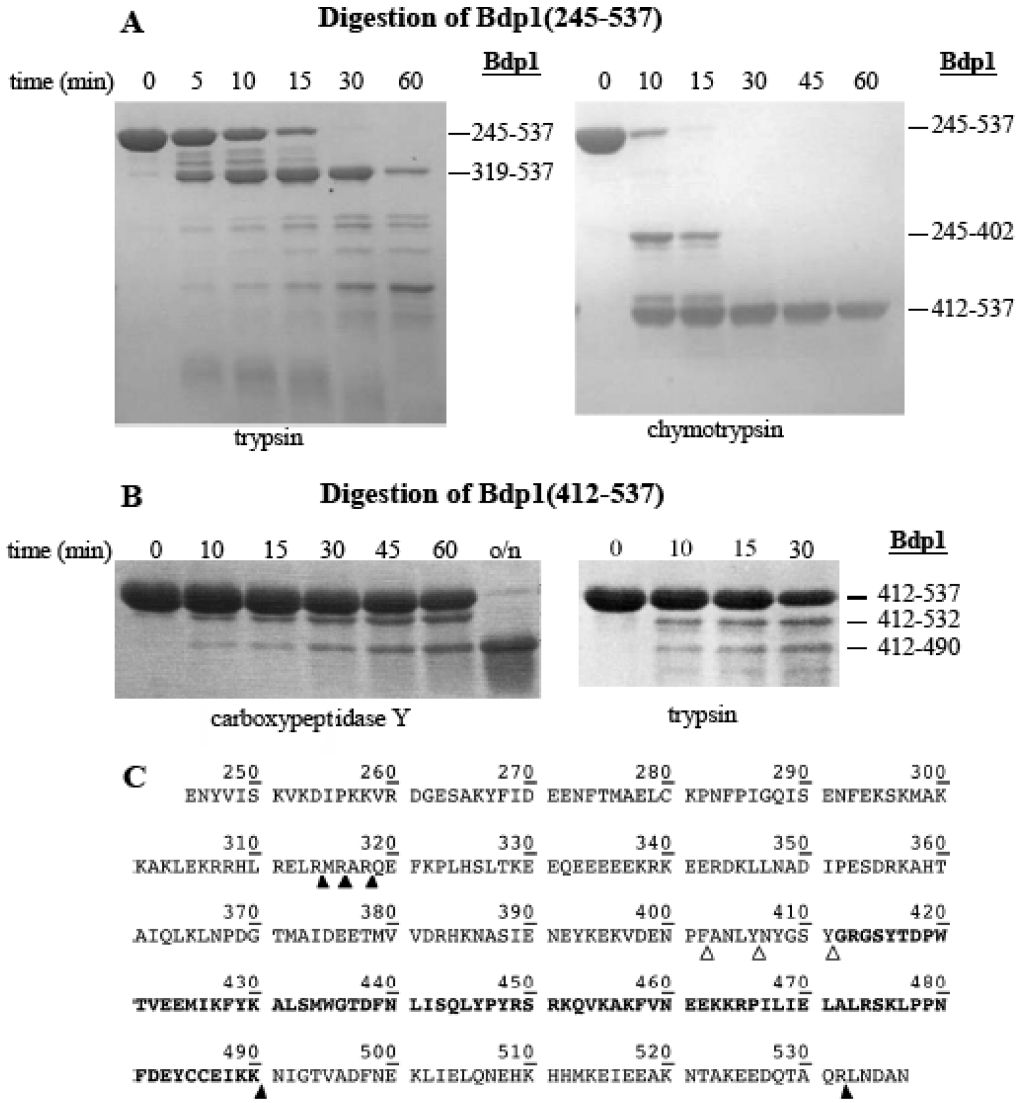

FIGURE 1: Limited proteolysis of Bdp1 by trypsin, chymotrypsin, and carboxypeptidase Y. (A) Time course of the proteolysis of Bdp1(245−537) with trypsin (left) and chymotrypsin (right). (B) Time course of proteolysis of Bdp1(412−537) with carboxypeptidase Y (left; o/n, overnight with 5-fold less enzyme) and trypsin (right). Identified products are specified to the right of each image. (C) Sequence of Bdp1(245−537) showing trypsin (▲) and chymotrypsin (△) cleavage sites that were identified by mass spectrometry and N-terminal sequencing. The highlighted sequence corresponds to the smallest protease-resistant fragment.

of Bdp1 did not significantly differ from the locations in these representative SANT domains. The only noteworthy secondary structure difference is the significantly shorter α2 helix of Bdp1.

NMR Titration of the Backbone of Bdp1 with Unlabeled Brf1. A previously published study showed that Bdp1(410−476) is essential for binding to the C-terminal one-third of Brf1 [Brf1(439−596)]; an additional contribution to the interaction is provided by the Bdp1(477−492) segment (*6*). The study, based on a collection of Bdp1 internal deletions, failed to identify the relative contribution of each Bdp1 amino acid in the binding of Brf1. Here, using the chemical shift perturbation of $^{15}N-^{1}H$ HSQC cross-peaks (*18*), I assessed the binding propensity of Bdp1(412−493) for Brf1(439−544) and possible changes in the chemical environment of the backbone amide for each Bdp1 residue. Brf1(439−544) contains the main binding site of Brf1 to Bdp1 (*6*), and its relatively small size permits a spectroscopic study of Bdp1 without a dramatic loss of the NMR signal. The titration of the Bdp1(412−493) $^{15}N-^{1}H$ cross-peaks with unlabeled Brf1(439−544) is described in Experimental Procedures. To decrease the level of nonspecific interactions, the binding buffer contained a moderate concentration of NaCl (200 mM) and a high concentration of arginine and glutamic acid (50 mM each) serving as nonspecific competitors (*19*). The Bdp1(412−493) concentration was 400 μM, and Brf1(439−544) was titrated from 50 to 200 μM.

The shift of Bdp1(412−493) HSQC cross-peaks by 200 μM Brf1(439−544) is quantified in Figure 3 (excluding prolines; residues 471−473 and 487 were not assigned). Five cross-peaks were strongly shifted ($\Delta > 0.025$): K430, Q444, Y448, R465, and K489. Residues with modest changes ($0.015 < \Delta < 0.025$) are also identified in the figure since their signals are distinguishable from background noise (estimated at ~0.0075 ppm). Chemical shift perturbations can result either from direct, localized interaction or from gross conformational changes in the labeled partner. The paucity of significantly perturbed residues and their isolation from adjacent residues in Figure 3 strongly argue against a major conformational change in Bdp1(412−493). Figure 4A shows an example

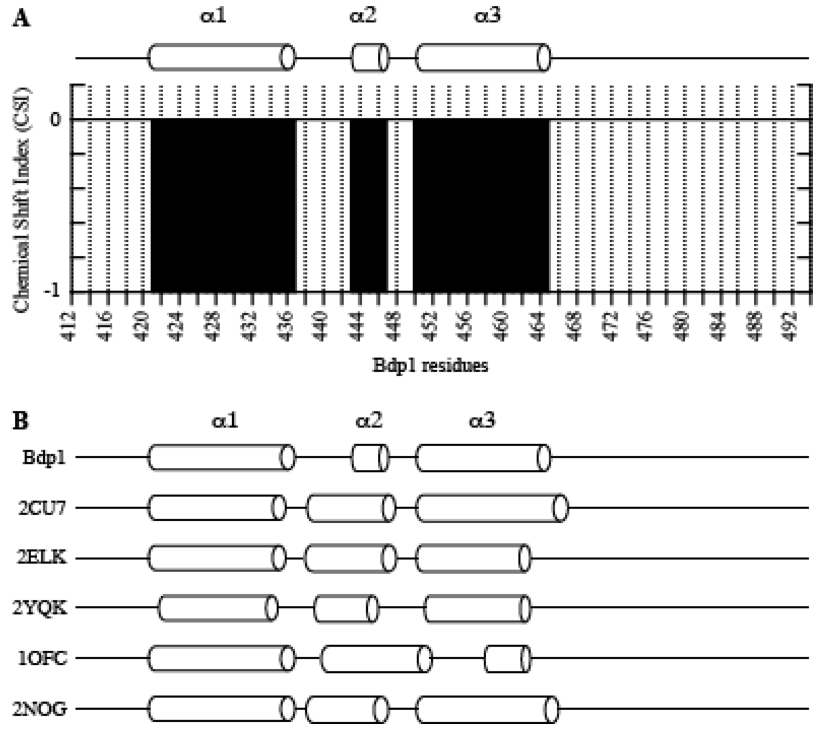

FIGURE 2: NMR-derived secondary structure of Bdp1(412−493). (A) Chemical shift index of $^{1}H^{\alpha}$, $^{13}C^{\alpha}$, $^{13}C^{\beta}$, and $^{13}C'$ nuclei (as calculated with CSI 2.1) showing the position of helices α1−α3. (B) Secondary structure comparison of Bdp1(412−493) with five representative SANT domains. α-Helices are represented as tubes, as assigned in the Protein Data Bank entries specified at the left.

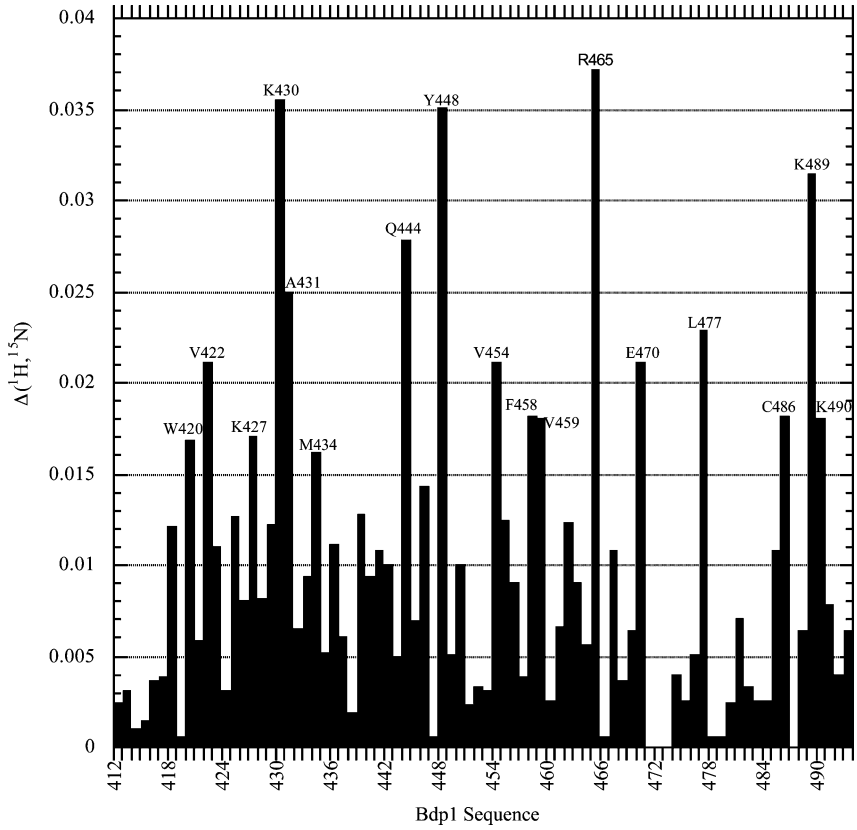

FIGURE 3: Chemical shift perturbation of Bdp1(412−493) $^{15}N-^{1}H$ HSQC cross-peaks by unlabeled Brf1(439−544). Protein concentrations were 400 μM (Bdp1) and 200 μM (Brf1). $\Delta(^{1}H,^{15}N) = [(\delta\sigma_H)^2 + (\delta\sigma_N/10)^2]^{1/2}$. $\delta\sigma_H$ and $\delta\sigma_N$ are the differences, in parts per million, of the proton and nitrogen chemical shifts, respectively. Cross-peaks for residues 471−473 and 487 were not assigned. The mean $\Delta(^{1}H,^{15}N)$ of all Bdp1 cross-peaks was 0.010; cross-peaks with a $\Delta(^{1}H,^{15}N)$ of >0.02 are considered significant and identified in the graph along with cross-peaks of possible significance ($0.02 > \Delta > 0.015$).

of cross-peak displacement (R465, red trace) as Brf1 is titrated from 50 μM (dark blue) to 200 μM (white), notably with negligible line broadening. The fact that an adjacent cross-peak corresponding to residue S415 is not significantly altered by Brf1 strongly supports the specificity of the measured chemical shift perturbations.

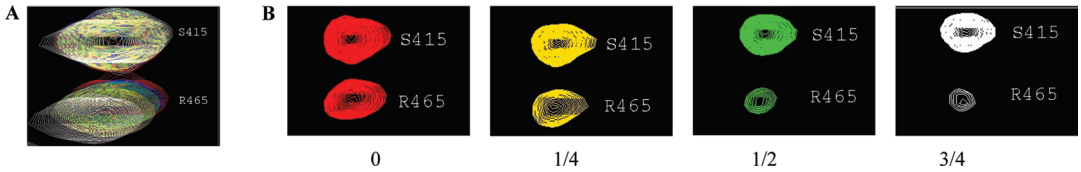

FIGURE 4: Response of the $^{15}N-^{1}H$ HSQC cross-peak of Bdp1 residue R465 to addition of unlabeled Brf1(439−544) or TBPc-Brf1(439−544). (A) Superposition of the R465 and S415 cross-peaks when increasing amounts of unlabeled Brf1(439−544) are added (Brf1:Bdp1 ratios of 0, 1:16, 1:8, 1:4, and 1:2 in red, blue, turquoise, yellow, and white, respectively). (B) Evolution of the R465 and S415 cross-peaks when increasing amounts of TBPc-Brf1(439−544) are added at Brf1−TBP:Bdp1 ratios of 0, 1:4, 1:2, and 3:4.

I next examined if any of these interactions between Bdp1 and Brf1 in the binary TFIIIB subcomplex are maintained in the context of a ternary TFIIIB complex (i.e., when TBP is also present). For this purpose, the transcriptionally competent TBP(61−240)−-Brf1(439−544) fusion protein [TBP(61−240) is the evolutionarily conserved core domain of yeast TBP] (*6*) was used for the $^{15}N-^{1}H$ HSQC Bdp1 cross-peak perturbation assay. Figure 4B shows that, when TBPc-Brf1(439−544) was titrated, the NMR signal of R465 (but not S415) was progressively lost without the appearance of a new cross-peak. This loss of signal can be explained by the dramatic increase in the molecular size of Bdp1 [from ∼10 kDa in the free form to ∼50 kDa in the TBPc-Brf1(439−544)-bound form]. Similar results were obtained for K430, Q444, Y448, and K489 (data not shown).

Brf1/Bdp1 Pull-Down Assay. To examine whether the NMR-detected interaction between Bdp1 and Brf1 fragments could also be observed in solution under nonequilibrium conditions, a pull-down assay was designed. This assay exploits the high affinity of Bdp1(412−493) for heparin−agarose beads (elution does not occur below 600 mM NaCl) and the inability of Brf1(439−544) to bind to the same beads above 150 mM NaCl. Bdp1(412−493) and increasing concentrations of Brf1(439−544) were incubated in buffer containing 200 mM NaCl, 50 mM arginine, and 50 mM glutamic acid and applied to heparin−agarose beads. After several washes, Bdp1(412−493) and any retained Brf1(439−544) were eluted with 1 M NaCl and analyzed by SDS−PAGE. The results are shown in Figure 5. Despite the nonequilibrium conditions of the assay, increasing amounts of Brf1(439−544) coelute with Bdp1(412−493), but at substoichiometric levels even when Brf1 is added at a 5-fold molar excess relative to Bdp1. This indicates a weak interaction between Bdp1(412−493) and Brf1(439−544), with a dissociation constant between 26 μM [top panel; with the wash fractions considered bound, ∼50% of the loaded Brf1(439−544) is in the FT fraction] and 130 μM (bottom panel; with the wash fractions considered unbound, the molar level of Brf1 is $^{2}/_{3}$ of that of Bdp1 in the E1 fraction), consistent with the observation that TFIIIB dissociates into Bdp1 and Brf1−TBP subcomplexes during chromatographic purification (*1*).

Backbone Assignment and Secondary Structure of Brf1(439−544). Having assigned the backbone of Bdp1(412−493) and mapped its contacts with Brf1(439−544), I undertook the reciprocal task of assigning the backbone of Brf1 and mapping its contacts with Bdp1. Brf1(439−544) was uniformly labeled with ^{15}N and purified under native conditions, and its $^{15}N-^{1}H$ HSQC spectrum was recorded in the NMR buffer at 25 °C (see Figure S1 of the Supporting Information). Brf1(439−544) cross-peaks were seen to be sharp, with high signal-to-noise ratios; intensities were evenly distributed and accounted for all amide pairs of the backbone. The

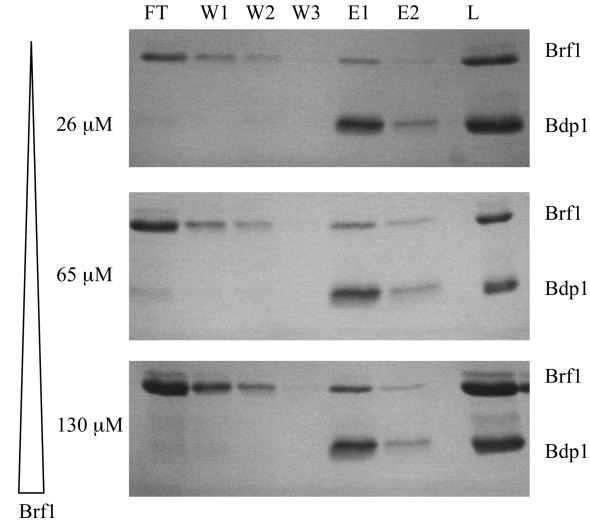

FIGURE 5: Brf1/Bdp1 pull-down assay using heparin−agarose beads. Bdp1(412−493) (25 μM) was incubated with increasing concentrations of Brf1(439−544) and chromatographed on heparin−agarose beads (see Experimental Procedures for details). FT, flow-through; W1−W3, column washes; E1 and E2, high-salt elution; L, total protein before chromatography.

narrow chemical shift window in the proton dimension (∼1 ppm for non-side chain cross-peaks) indicates that the protein does not adopt a compact three-dimensional fold (*20*−*24*). Next, Brf1(439−544) was uniformly labeled with ^{13}C and ^{15}N and purified under native conditions, and its backbone resonances were assigned using multidimensional NMR. The secondary structure of Brf11(440−544) was derived using the chemical shift index of $^{1}H^{\alpha}$, $^{13}C^{\alpha}$, $^{13}C^{\beta}$, and $^{13}C'$ nuclei. In partially folded proteins, chemical shift deviations from their random coil values can arise not only from residual secondary structures but also from local sequence effects. Accordingly, the CSI-derived secondary structure of Brf1-(439−544) was confirmed by computing the secondary chemical shift of $^{13}C'$ to include sequence-dependent corrections of random coil NMR chemical shifts (*12, 25*). The results are presented in Figure 6A.

Brf1(439−544) folds into seven short helices (α1−α7), with α1, α2, and α4 being the shortest (Figure 6A). These helices were compared to their counterparts in the crystal structure of Brf1(439−596) bound to TBP and DNA (*4*), of which Brf1 residues 439−506 and 454−506, respectively, were resolved in only two of the four Brf1 molecules present in the asymmetric unit (Figure 6B). Whereas helices α1 and α2 correspond well to helices H20 (not named in ref *4*) and H21 in the crystal structure, the counterpart of helices H22, H23, and H24 is helix α3 of the NMR structure. H25 is absent from the NMR structure, with the junction between H24 and H25 corresponding to

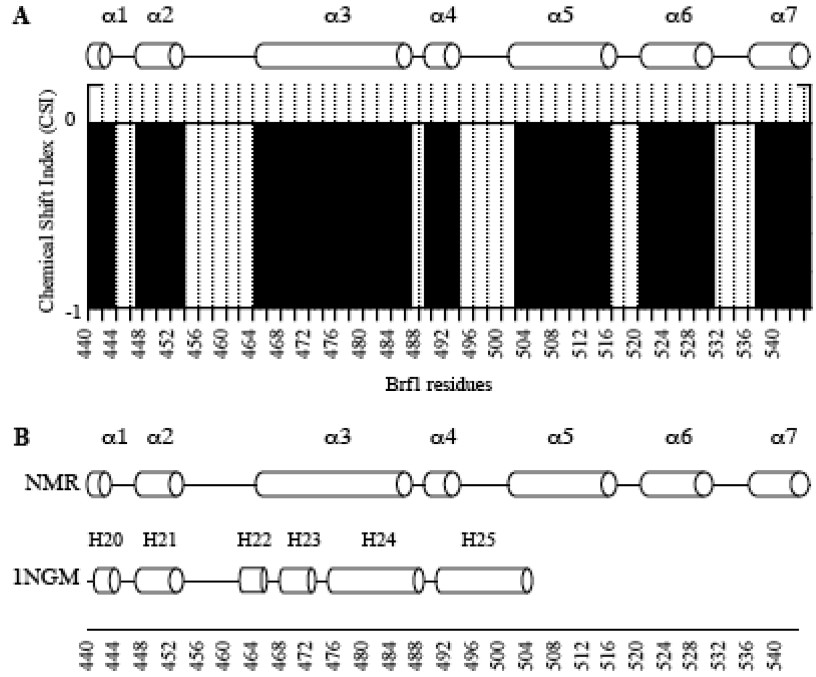

FIGURE 6: NMR-derived secondary structure of Brf1(439−544). (A) Chemical shift index of $^{1}H^{\alpha}$, $^{13}C^{\alpha}$, $^{13}C^{\beta}$, and $^{13}C'$ (as calculated with CSI 2.1) showing the position of helices α1−α7. (B) Alignment of the NMR-derived secondary structure of Brf1(439−544) with that of the Brf1 439−506 segment resolved in the Brf1(439−596)−TBP−DNA crystal (PDB entry 1NGM).

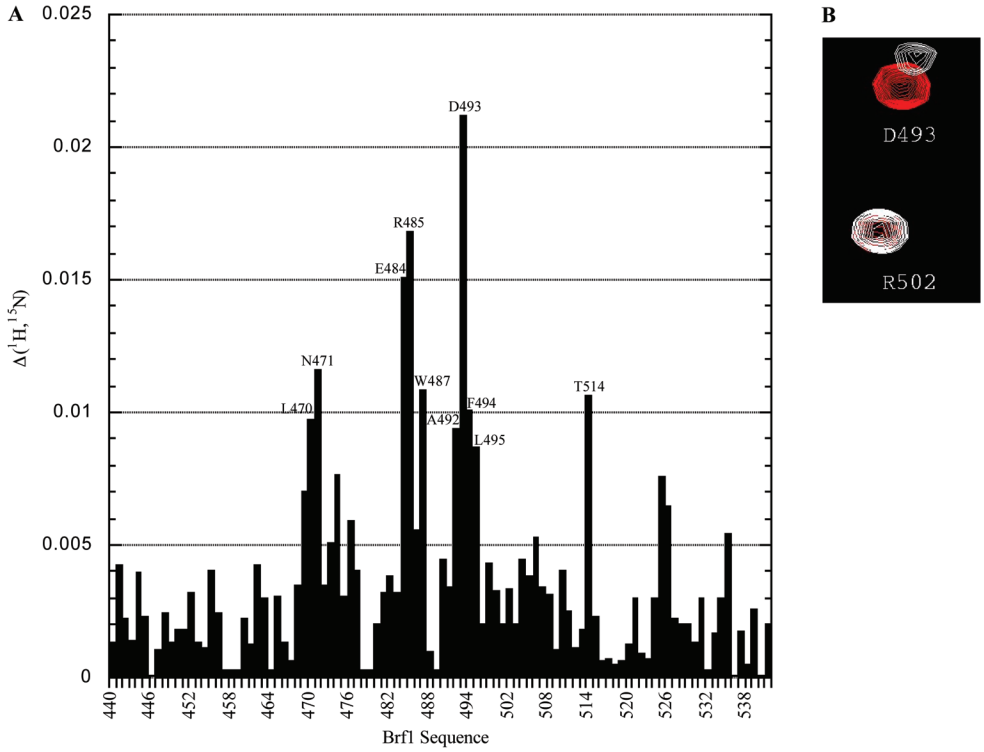

FIGURE 7: Chemical shift perturbation of Brf1(439−544) $^{15}N-^{1}H$ HSQC cross-peaks by unlabeled Bdp1(412−493). (A) Protein concentrations were 300 μM (Brf1) and 150 μM (Bdp1). $\Delta(^{1}H,^{15}N)$ as defined for Figure 3. The mean $\Delta(^{1}H,^{15}N)$ of all Brf1 cross-peaks was 0.0036; cross-peaks with a $\Delta(^{1}H,^{15}N)$ of >0.08 are considered significant and identified in the graph. (B) Superposition of the D493 and R502 cross-peaks in the absence of Bdp1 (red) and in its presence (white; Bdp1:Brf1 ratio of 1:2).

helix α4. Helices α5−α7 correspond to a Brf1 segment that was not resolved in the crystal structure.

Brf1 Residues Interacting with Bdp1. The shift of each Brf1 $^{15}N-^{1}H$ HSQC cross-peak when unlabeled Bdp1-(412−493) was added is shown in Figure 7A (at a Bdp1:Brf1 molar ratio of 1:2; see Experimental Procedures). R484, R485, and D493 cross-peaks were significantly perturbed, suggesting strong involvement in the Bdp1 interaction. L470, N471, W487, A492, F494, L495, and T514 cross-peaks were also perturbed, but to a lesser extent. Figure 7B shows an example of the D493 cross-peak displacement caused by Bdp1-(412−493). The neighboring cross-peak of R502 was not altered.

Effect of TBP on the Conformation of Brf1. The distribution of HSQC cross-peaks along the proton and nitrogen dimensions provides a way to assess whether TBP(61−240)

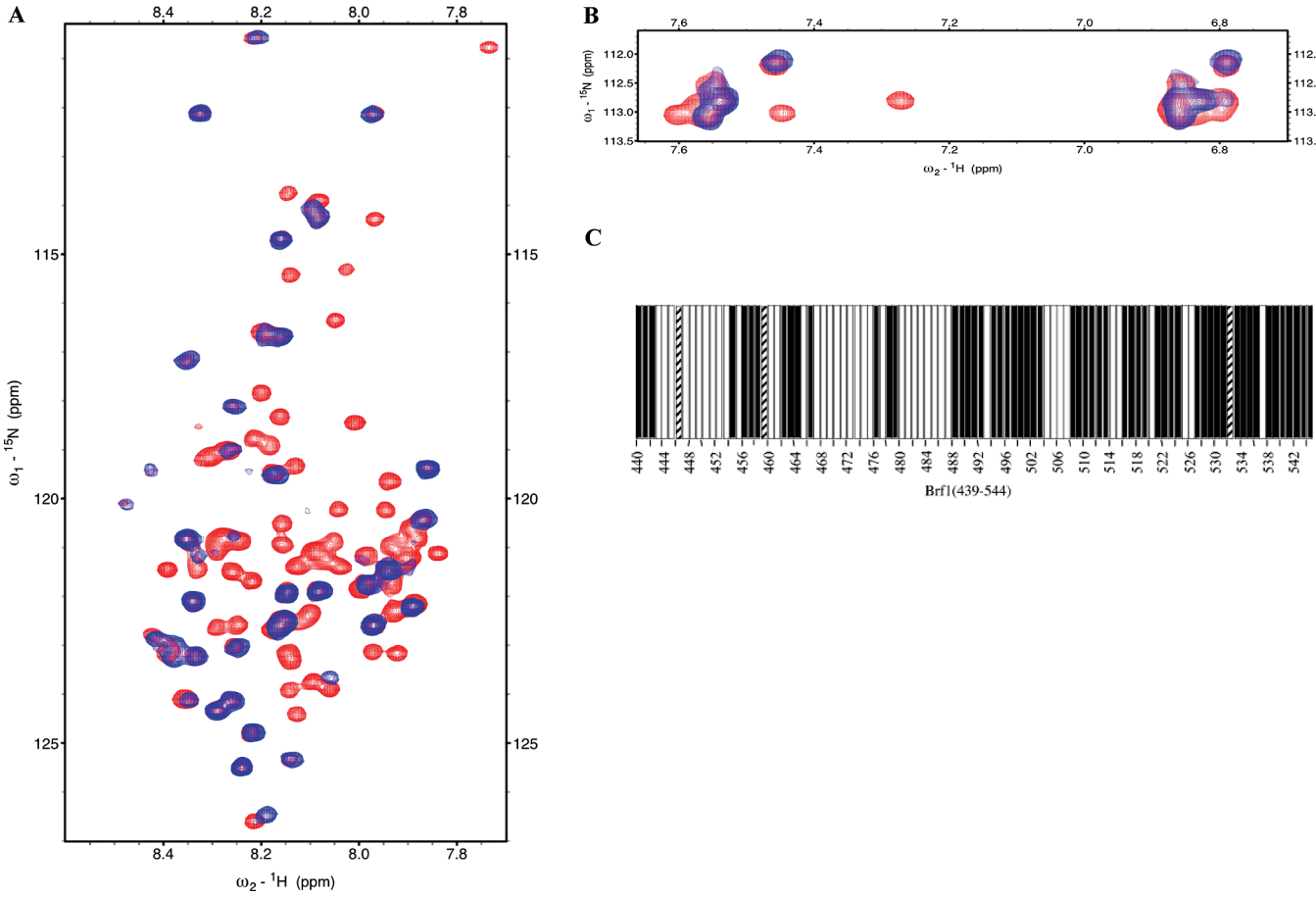

FIGURE 8: Superposition of the ^{15}N−^{1}H HSQC spectra of unbound Brf1(439−544) (red) and Brf1(439−544) bound to TBPc (blue). The TBPc:Brf1 ratio is 1:1: (A) main spectrum and (B) the amide region for the side chains of glutamine and asparagine. (C) Brf1 cross-peaks that remain unperturbed (black bars) or disappear (white bars) in the presence of TBPc. Brf1 prolines are indicated (hatched bars).

binding causes dramatic three-dimensional changes in the structure of Brf1(439−544). Brf1(439−544) binds to TBP−DNA complexes with high affinity (K_D < 50 nM) (*26*) with no evidence of DNA contributing to this interaction (*4*). Dissociation of the TBP−Brf1 complex should be very slow with respect to the NMR time scale such that cross-peaks of Brf1 amides at the interacting interface will be either fully shifted or entirely unchanged at substoichiometric levels of TBP. Figure 8 (panels A and B) superimposes the HSQC spectra of free Brf1 (red) and Brf1 bound to TBP (blue): 57 of the 100 amide cross-peaks remain visible in the spectrum after addition of TBP, with only modest changes in their respective chemical shifts; the remaining 43 cross-peaks disappear without the emergence of new, shifted cross-peaks. I interpret residues corresponding with absent cross-peaks to be interacting directly with TBP (or conformationally altered by that interaction), with line broadening obscuring the bound-state cross-peak in the larger complex (~33 kDa). The evolution of particular Brf1 cross-peaks as unlabeled TBP is titrated is shown in Figure S2 of the Supporting Information. The Brf1 cross-peaks that are maintained or disappear upon addition of TBP are summarized in Figure 8C. Thirty-two of the 57 Brf1 cross-peaks that remain upon addition of TBP reside in the Brf1 segment encompassing helices α5−α7 that are not involved in TBP interaction or not resolved in the TBPc−Brf1(439−596)−DNA crystal structure (*4*). The maintenance or loss status of cross-peaks between residues 440 and 487 is largely consistent with the crystal structure, with the possible exception of maintained cross-peaks corresponding to residues 456−458 between helices α2 and α3, which make numerous contacts with TBP. The most striking difference involves the segment encompassing helix α4 and the N-terminal half of helix α5. The maintenance of cross-peaks corresponding to residues 488−503 indicates that helices α4 and α5 are maintained and do not rearrange to form the crystal structure helix H25 in the absence of DNA, while the multiple contacts that residue 494 makes with TBP in the crystal structure are probably absent. Instead, the loss of cross-peaks corresponding to residues 504−508 (that are not proximal to TBP in the crystal structure) may signify an alternative interaction.

DISCUSSION

Digestion of the C-terminal half of Bdp1 with trypsin and chymotrypsin revealed a protease-resistant segment that corresponds to Bdp1(412−493). This segment contains the SANT domain, the most conserved sequence in Bdp1. When expressed in *E. coli,* Bdp1(412−493) is insoluble, suggesting that this minimal segment fails to fold correctly. Adding Bdp1 segment 319−411 makes the protein fully soluble (Figure S3 of the Supporting Information). Similarly, adding Bdp1 residues C-terminal to position 493 gradually increases solubility. This suggests that the protease-resistant Bdp1-(412−493) segment engages in interactions with upstream and downstream residues that are significant for the folding pathway of Bdp1.

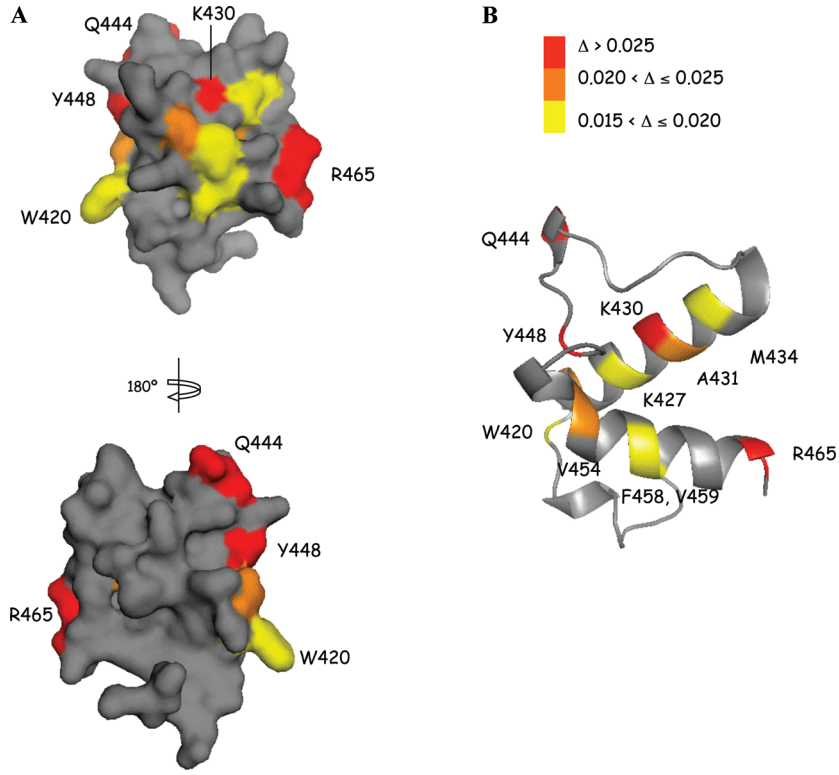

FIGURE 9: NMR-derived model of the three-dimensional structure of Bdp1(412−466) showing residues perturbed by the addition of Brf1(439−544). Surface (A) and cartoon (B) views are shown. Significantly perturbed Bdp1 residues with $\Delta(^1H,^{15}N)$ of >0.025 ppm or between 0.025 and 0.020 ppm are colored red and orange, respectively. Residues with potentially significant Δ values [0.020 > $\Delta(^1H,^{15}N)$ > 0.015 ppm] are colored yellow.

Assignment of the backbone of Bdp1(412−493) was achieved using multidimensional heteronuclear NMR. Secondary structure assignments show that this segment of Bdp1 contains a canonical, three-helix, SANT domain encompassing residues 412−465. CSI calculations showed that the protease-resistant 466−493 segment is nevertheless devoid of recognizable (i.e., α-helix/β-strand) secondary structure. I suggest that this segment might wrap in an extended but structurally constrained conformation on its SANT domain core.

The NMR-derived secondary structure of Brf1(439−544) contains seven short helices (α1−α7). Helices α1−α4 partially coincide with counterparts in the crystal structure of a DNA−TBP−Brf1 ternary complex (*4*). These short helical segments probably fluctuate between random coil and helical structures with the CSI-derived secondary structure representing an ensemble average. This idea is supported by the fact that the crystal structure of the DNA−TBP−Brf1 ternary complex (PDB entry 1NGM) shows a unit cell containing four distinct Brf1 molecules (namely, B, F, J, and N) in which the position of the α-helices does not completely coincide (Figure S4 of the Supporting Information).

Three Brf1 residues (E484, R485, and D493) are significantly shifted upon the binding of Bdp1. A more modest shift is observed with residues L470, N471, W487, A492, F494, L495, and T514. When these residues are artificially transposed on the crystal structure of Brf1 bound to TBP and DNA (see Figure S5 of the Supporting Information), R485 and E484 are found (as one would expect) completely pointing away from TBP. The same Figure S5 shows, however, that the significantly shifted residue D493 has maintained a relatively close orientation with regard to TBP. This suggests that for at least this residue, the three-dimensional locations in a Brf1−Bdp1 binary complex and in a Brf1−TBP−DNA ternary complex do not necessarily coincide.

When Bdp1 (25 μM) is used as bait, the heparin pull-down assay showed that a 5-fold molar excess of Brf1 over Bdp1 yields only a small, substochiometric, fraction of Brf1 bound to Bdp1. This observation can be interpreted by a high dissociation constant between Bdp1(412−493) and Brf1-(439−544), possibly originating from a fast dissociation rate. The dissociation constant for the Bdp1(412−493)−Brf1-(438−544) interaction (as measured from concentration-dependent chemical shift changes) is on average 258 μM (146 μM for Bdp1 residue R465 and 370 μM for Bdp1 residue K430). Figure S6 of the Supporting Information shows a plot of these chemical shift changes for Bdp1 residues R465 and K430 as unlabeled Brf1 is titrated up. There are no published values for the dissociation constant between isolated full-length Bdp1 and full-length Brf1. However, the apparent dissociation constant between full-length Bdp1 and Brf1 as assembled in the TFIIIB complex (i.e., in the presence of TBP and DNA) can be estimated from gel shifts and cross-linking experiments to be roughly in the ∼100 nM range (*6, 7, 26*). That this value is several orders of magnitude higher than the value obtained for the minimal Bdp1(412−493)−Brf1(439−544) complex is not surprising. Indeed, recruitment of Bdp1 to the TFIIIB complex does not exclusively rely on its interaction with Brf1 through the SANT domain. There are multiple sites of interaction between Bdp1 and the DNA−TBP−Brf1 com-

plex, including direct interactions of Bdp1 with DNA (*6, 7, 26*). Furthermore, in the context of a TFIIIB complex, DNA-bound TBP interacts strongly with Brf1 and increases the local concentration of Brf1 molecules available for binding Bdp1, hence increasing the apparent dissociation constant between Bdp1 and Brf1.

The addition of unlabeled TBP to ^{15}N-labeled Brf1-(439−544) caused the disappearance of a large number of Brf1 HSQC cross-peaks, indicating that Brf1(439−544) shares an extensive interaction interface with TBP in the absence of DNA. The effects of TBP on Brf1 cross-peaks corresponding to residues 440−487 are generally consistent with interactions seen in the crystal structure of a TBP−Brf1 complex that contains DNA (*4*). However, the maintenance of cross-peaks for Brf1 residues S456−D458, which together contribute five hydrogen bonds with TBP convex surface residues, suggests that the conformation of this region in the crystal structure is not established in the absence of DNA and/or Brf1 residues 545−596. Double-alanine substitution of D457 and D458 did not have a detectable phenotype in vivo (*27*), suggesting that some conformational flexibility is allowed in this region. The maintenance of cross-peaks for Brf1 residues 488−503 implies that helix H25 of the Brf1 crystal structure is also not established in the absence of DNA and/or Brf1 residues 545−596. Although not resolved in the Brf1(439−596)−TBP−DNA crystal structure, the Brf1 510−596 segment contains a nonspecific DNA binding activity that is not manifested in full-length Brf1 alone (*28*), and removal of this Brf1 segment reduces the efficiency of Brf1−DNA cross-linking in Brf1−TBP−DNA complexes (*6*). This suggests the possibility that the existence and orientation of helix H25 in the crystal structure are dependent on an unresolved Brf1−DNA interaction.

A model of the three-dimensional structure of Bdp1(412−465) (Figure 9) was built by threading the experimentally measured chemical shifts into a structural database that excludes highly homologous proteins (*14*). NMR titration of the Bdp1 backbone showed that K430, Q444, Y448, R465, and K489 are strongly perturbed upon binding of Brf1(439−544) (Y448 and R465 are in the model and colored red) with perturbation of the cross-peaks corresponding to V422, A431, V454, E470, and L477 also likely to be significant (V422, A431, and V454 are in the model and colored orange). These Brf1-perturbed Bdp1 residues cluster broadly on one face of the protein (panel A), suggesting a convex interaction surface from R465 to Q444. This protein-binding interface, mainly formed by helix 1 and helix 3 (panel B), differs from the DNA binding surface previously described for related SANT/MYB domains. In those structures, helices 2 and 3 form a canonical helix−turn−helix motif in which helix 3 recognizes DNA by packing into the major grove (*29*). This finding suggests that despite its relative simplicity, the same trihelical SANT domain can accommodate at least two distinct biological functions by interacting with its ligands through a specific pair of helices.

ACKNOWLEDGMENT

I thank Matthew Williamson, Justin Torpey, Xuemei Huang, and Dexin Deng for outstanding technical assistance with N-terminal protein sequencing, mass spectrometry, NMR, and protein purification, respectively. I'm grateful to George Kassavetis for providing some of the expression vectors used in this study, for incisive comments and discussions, and for carefully editing the text and some of the figures. General support to this work and permission to publish are acknowledged (E. Peter Geiduschek).

SUPPORTING INFORMATION AVAILABLE

Five supporting figures (S1−S5). This material is available free of charge via the Internet at http://pubs.acs.org.

REFERENCES

1. Kassavetis, G. A., and Geiduschek, E. P. (2006) Transcription factor TFIIIB and transcription by RNA polymerase III. *Biochem. Soc. Trans. 34*, 1082–1087.
2. Geiduschek, E. P., and Kassavetis, G. A. (2006) Transcription: Adjusting to adversity by regulating RNA polymerase. *Curr. Biol. 16*, R849–R851.
3. Schramm, L., and Hernandez, N. (2002) Recruitment of RNA polymerase III to its target promoters. *Genes Dev. 16*, 2593–2620.
4. Juo, Z. S., Kassavetis, G. A., Wang, J., Geiduschek, E. P., and Sigler, P. B. (2003) Crystal structure of a transcription factor IIIB core interface ternary complex. *Nature 422*, 534–539.
5. Aasland, R., Stewart, A. F., and Gibson, T. (1996) The SANT domain: A putative DNA-binding domain in the SWI-SNF and ADA complexes, the transcriptional co-repressor N-CoR and TFIIIB. *Trends Biochem. Sci. 21*, 87–88.
6. Kassavetis, G. A., Driscoll, R., and Geiduschek, E. P. (2006) Mapping the principal interaction site of the Brf1 and Bdp1 subunits of *Saccharomyces cerevisiae* TFIIIB. *J. Biol. Chem. 281*, 14321–14329.
7. Kassavetis, G. A., Soragni, E., Driscoll, R., and Geiduschek, E. P. (2005) Reconfiguring the connectivity of a multiprotein complex: Fusions of yeast TATA-binding protein with Brf1, and the function of transcription factor IIIB. *Proc. Natl. Acad. Sci. U.S.A. 102*, 15406–15411.
8. Saida, F., Odaert, B., Uzan, M., and Bontems, F. (2004) First structural investigation of the restriction ribonuclease RegB: NMR spectroscopic conditions, ^{13}C/^{15}N double-isotopic labelling and two-dimensional heteronuclear spectra. *Protein Expression Purif. 34*, 158–165.
9. Markley, J. L., Bax, A., Arata, Y., Hilbers, C. W., Kaptein, R., Sykes, B. D., Wright, P. E., and Wuthrich, K. (1998) Recommendations for the presentation of NMR structures of proteins and nucleic acids. IUPAC-IUBMB-IUPAB Inter-Union Task Group on the Standardization of Data Bases of Protein and Nucleic Acid Structures Determined by NMR Spectroscopy. *J. Biomol. NMR 12*, 1–23.
10. Jung, Y. S., and Zweckstetter, M. (2004) Mars: Robust automatic backbone assignment of proteins. *J. Biomol. NMR 30*, 11–23.
11. Wishart, D. S., and Sykes, B. D. (1994) The ^{13}C chemical-shift index: A simple method for the identification of protein secondary structure using ^{13}C chemical-shift data. *J. Biomol. NMR 4*, 171–180.
12. Schwarzinger, S., Kroon, G. J., Foss, T. R., Chung, J., Wright, P. E., and Dyson, H. J. (2001) Sequence-dependent correction of random coil NMR chemical shifts. *J. Am. Chem. Soc. 123*, 2970–2978.
13. Sugase, K., Dyson, H. J., and Wright, P. E. (2007) Mechanism of coupled folding and binding of an intrinsically disordered protein. *Nature 447*, 1021–1025.
14. Wishart, D. S., and Case, D. A. (2001) Use of chemical shifts in macromolecular structure determination. *Methods Enzymol. 338*, 3–34.
15. Willard, L., Ranjan, A., Zhang, H., Monzavi, H., Boyko, R. F., Sykes, B. D., and Wishart, D. S. (2003) VADAR: A web server for quantitative evaluation of protein structure quality. *Nucleic Acids Res. 31*, 3316–3319.
16. Olsen, J. V., Ong, S. E., and Mann, M. (2004) Trypsin cleaves exclusively C-terminal to arginine and lysine residues. *Mol. Cell. Proteomics 3*, 608–614.
17. Appel, W. (1986) Chymotrypsin: Molecular and catalytic properties. *Clin. Biochem. 19*, 317–322.
18. Zuiderweg, E. R. (2002) Mapping protein-protein interactions in solution by NMR spectroscopy. *Biochemistry 41*, 1–7.

19. Golovanov, A. P., Hautbergue, G. M., Wilson, S. A., and Lian, L. Y. (2004) A simple method for improving protein solubility and long-term stability. *J. Am. Chem. Soc. 126*, 8933–8939.
20. Yao, J., Dyson, H. J., and Wright, P. E. (1997) Chemical shift dispersion and secondary structure prediction in unfolded and partly folded proteins. *FEBS Lett. 419*, 285–289.
21. Mittag, T., and Forman-Kay, J. D. (2007) Atomic-level characterization of disordered protein ensembles. *Curr. Opin. Struct. Biol. 17*, 3–14.
22. Eliezer, D. (2007) Characterizing residual structure in disordered protein states using nuclear magnetic resonance. *Methods Mol. Biol. 350*, 49–67.
23. Dyson, H. J., and Wright, P. E. (1998) Equilibrium NMR studies of unfolded and partially folded proteins. *Nat. Struct. Biol. 5* (Suppl.), 499–503.
24. Barbar, E. (1999) NMR characterization of partially folded and unfolded conformational ensembles of proteins. *Biopolymers 51*, 191–207.
25. Schwarzinger, S., Kroon, G. J., Foss, T. R., Wright, P. E., and Dyson, H. J. (2000) Random coil chemical shifts in acidic 8 M urea: Implementation of random coil shift data in NMRView. *J. Biomol. NMR 18*, 43–48.
26. Kassavetis, G. A., Kumar, A., Ramirez, E., and Geiduschek, E. P. (1998) Functional and structural organization of Brf, the TFIIB-related component of the RNA polymerase III transcription initiation complex. *Mol. Cell. Biol. 18*, 5587–5599.
27. Andrau, J. C., Sentenac, A., and Werner, M. (1999) Mutagenesis of yeast TFIIIB70 reveals C-terminal residues critical for interaction with TBP and C34. *J. Mol. Biol. 288*, 511–520.
28. Huet, J., Conesa, C., Carles, C., and Sentenac, A. (1997) A cryptic DNA binding domain at the COOH terminus of TFIIIB70 affects formation, stability, and function of preinitiation complexes. *J. Biol. Chem. 272*, 18341–18349.
29. Ogata, K., Morikawa, S., Nakamura, H., Sekikawa, A., Inoue, T., Kanai, H., Sarai, A., Ishii, S., and Nishimura, Y. (1994) Solution structure of a specific DNA complex of the Myb DNA-binding domain with cooperative recognition helices. *Cell 79*, 639–648.

BI801406Z